Check for updates

Geophysical Research Letters

RESEARCH LETTER
10.1029/2026GL121813

The Detection of Transient Subduction Zone Interface Properties Using Teleseismic Data

F. Rappisi[1,2], **T. J. Craig**[1,3], **and S. Rost**[1]

[1]School of Earth and Environment, University of Leeds, Leeds, UK, [2]Now at European Center for Geodynamics and Seismology, Walferdange, Luxembourg, [3]COMET, School of Earth and Environment, University of Leeds, Leeds, UK

Key Points:

- Remote seismological observations reveal slow slip potential in subduction zones
- Megathrust reflectors and fluid-driven processes correlate with slow slip events
- Proposed seismic method extends the study of inaccessible offshore subduction interfaces

Supporting Information:

Supporting Information may be found in the online version of this article.

Correspondence to:

F. Rappisi,
francescorappisi@gmail.com

Citation:

Rappisi, F., Craig, T. J., & Rost, S. (2026). The Detection of transient subduction zone interface properties using teleseismic data. *Geophysical Research Letters*, *53*, e2026GL121813. https://doi.org/10.1029/2026GL121813

Received 12 JAN 2026
Accepted 6 APR 2026

Author Contributions:

Conceptualization: T. J. Craig
Data curation: F. Rappisi
Formal analysis: F. Rappisi
Funding acquisition: T. J. Craig
Investigation: F. Rappisi
Methodology: F. Rappisi, T. J. Craig, S. Rost
Software: F. Rappisi
Supervision: T. J. Craig, S. Rost
Validation: F. Rappisi
Writing – original draft: F. Rappisi
Writing – review & editing: F. Rappisi

© 2026. The Author(s).
This is an open access article under the terms of the Creative Commons Attribution License, which permits use, distribution and reproduction in any medium, provided the original work is properly cited.

Abstract The physical properties of subduction zone interfaces govern the transition between stable aseismic slip, episodic slow slip events (SSEs), and large earthquakes. Ultraslow velocity layers (USVLs) along the megathrust are commonly interpreted as indicators of elevated pore-fluid pressures that promote slow slip, but their temporal variability remains poorly constrained, particularly offshore. Using the Mexican subduction zone as a test case, we show that seismic signatures consistent with USVLs can be detected using small-aperture seismic arrays at teleseismic distances. These high-reflectivity phases correlate spatially with independently documented SSEs, show temporal consistency with SSE occurrence and are absent outside SSE-prone regions. Our results suggest that slab geometry modulates fluid distribution along the megathrust and exerts a first-order control on slow slip occurrence. This study demonstrates a replicable, cost-effective approach to remotely probing transient megathrust properties, providing new opportunities to investigate offshore subduction zones where conventional geodetic observations are limited.

Plain Language Summary Subduction zones, where one tectonic plate slides beneath another, generate large earthquakes and tsunamis. Not all slip along these boundaries is sudden: some occurs slowly and aseismically in slow slip events (SSEs), often controlled by fluids along the plate interface. Detecting these events offshore is challenging because traditional instruments, like GPS, cannot easily monitor the deep ocean. Here, we show that small variations in seismic waves recorded at remote arrays can reveal ultra-slow velocity layers along the subduction interface. These layers indicate regions with elevated fluid content and are associated with slow slip. Using the Guerrero region in Mexico as a test case, we find that seismic detections of ultra-slow velocity layers align with the locations of known SSEs and vary in a way that is broadly consistent with their occurrence. Our approach provides a cost-effective, scalable method to monitor fluid-related processes and slow slip in subduction zones, improving our understanding of the seismic cycle and contributing to earthquake and tsunami hazard assessment in otherwise inaccessible offshore regions.

1. Introduction

The occurrence of episodic aseismic slip, where fault motion occurs at speeds too slow to radiate significant seismic energy, plays a crucial role in our understanding of subduction zone dynamics, particularly around the megathrust earthquake cycle, and the conditions leading to large major earthquakes and their associated tsunamis (Kato & Ben-Zion, 2021; Obara & Kato, 2016). The slow slip events (SSEs) provide a unique insight into the temporal balance of tectonics forces, the rheology of the subduction interface, and the mechanics of the megathrust. One major factor understood to govern the occurrence of such SSEs is the variation of pore fluid pressure along the subduction interface, with elevated fluid pressures in the megathrust believed to influence its stability and facilitate slow slip (Bürgmann, 2018; Song et al., 2009). Transient increases in pore fluid pressure likely result from progressive dehydration of subducted material, with released fluids migrating along a permeable interface and elevating pore pressures. These processes depend on the pressure-temperature evolution of the downgoing plate, its pre-subduction levels of hydration, and the permeability and geometry of the subduction interface. Interface permeability governs fluid residence time and its rheological impact.

SSEs predominantly occur in specific tectonic settings (e.g., Cascadia, Alaska, Japan, New Zealand, Mexico, Chile) where their spatial and temporal patterns are closely tied to the properties of the slab (Schwartz & Rokosky, 2007). For example, in the Guerrero region of Mexico, high fluid content in the flat segment of the slab is associated with frequent, short-term SSEs (S-SSEs), while in the steeper region of the slab, in close proximity to the coast, the presence of transient fluids triggers long-term SSEs (L-SSEs) (Frank et al., 2015; Radiguet

19448007, 2026, 8, Downloaded from https://agupubs.onlinelibrary.wiley.com/doi/10.1029/2026GL121813 by University Of Leeds The Brotherton Library, Wiley Online Library on [15/04/2026]. See the Terms and Conditions (https://onlinelibrary.wiley.com/terms-and-conditions) on Wiley Online Library for rules of use; OA articles are governed by the applicable Creative Commons License

et al., 2016). These observations illustrate the intricate interplay between slab geometry, mineralogy, pore pressure, and fluid distribution and dynamics. SSEs play an important role in accommodating strain in subduction zones, inducing cascading effects, relieving stress in the slipping zone while potentially increasing it in adjacent areas, sometimes triggering large earthquakes (Schwartz & Rokosky, 2007).

Modern geodetic techniques, particularly GPS/GNSS, have been pivotal in advancing our understanding of SSEs in subduction zones (Szeliga et al., 2008), providing valuable information about their timing, spatial extent, and the degree of interface coupling, based on the inversion of observed surface deformation. However, these methods rely primarily on onshore observations; seafloor geodesy remains limited, restricting investigations in fully submarine settings. Moreover, geodetic measurements are inherently kinematic and provide limited constraints on megathrust rheology.

Seismological techniques have also been employed to investigate SSEs, often focusing on the associated phenomena of tectonic tremor (TT) and low-frequency earthquakes (Ito et al., 2007; Schwartz & Rokosky, 2007)—small-scale patches of the interface slipping at rates sufficient to radiate low-frequency seismic waves. These studies typically require the deployment of dense local seismic arrays, often involving ocean-bottom seismometers, which are expensive and logistically challenging. In a pioneering study, Song et al. (2009) used near-field, local observations of small-magnitude earthquakes from beneath the megathrust in Southern Mexico, to observe *SP* converted phases—small-amplitude post-cursors to the direct *P* wave arrival, resulting from conversion from an upgoing *S* wave at the point where it transits the subduction interface, to reveal the presence of an ultra-slow velocity layer (USVL) atop the subducting plate. Their findings indicate that the spatial distribution of the USVL aligns with most slow slip patches, with these patches bounded by regions where the USVL is absent. This suggests that the USVL delineates the zone of transitional frictional behavior on the subduction interface. However, this study largely relied on detecting converted phases within the coda of direct arrivals from microearthquakes recorded at local distances. Whilst their main findings rely on local seismic stations in the near-field, Song et al. (2009) also demonstrated the potential to detect converted phases in far-field observations using array data, where they manifest as precursors to near-source reflections from the free surface (*pP* depth-phases). This approach potentially unlocks a new data set by leveraging the expanding seismic networks in many continental regions, enabling studies of subduction interface reflectivity on a global scale without dependence on local instrumentation.

Here, we build on that idea, utilizing remote seismic data to investigate the structure of the Mexican subduction zones. We develop an automated approach to determine if a reflected phase from a USVL is present (or is conclusively absent) between the direct *P* wave and the principal depth phase *pP* for shallow (<250 km depth) earthquakes occurring within the downgoing plate. We observe spatial and temporal variability in the detection (and absence) of these reflected phases, resulting from variations in the impedance properties of the subduction interface, inferred to result from the transient presence of fluids, and related to the occurrence of SSEs. This provides a cost-effective alternative to satellite-based geodesy and dense local seismic networks presenting a novel seismic observational framework to identify and monitor SSE-prone areas. By leveraging seismic array data recorded at teleseismic distances (30°–90°), we demonstrate the potential to infer slow slip processes and their underlying structural controls in subduction zones. This work not only has the potential to address a critical observational gap, but also introduces a replicable tool for advancing our understanding of tectonic processes, with implications for seismic and tsunami hazard assessment in underexplored marine environments.

2. HRI Phase Detection and Identification

Our approach relies on the ability to detect small-amplitude seismic phases at relatively high frequencies, observed at teleseismic distances from the earthquake source. In particular, we are interested in detecting depth-phase precursors (summarized in Figure 1a) resulting from the reflection of an up-going *P* wave at a high-impedance contrast, and therefore high reflectivity, subduction interface (termed HRI's hereafter). These HRI phases arrive between the direct *P* phase and its principal depth phase *pP* (Figure 1b), with the delay time relative to *P* resulting from the depth of the earthquake beneath the subduction interface, and the time by which a HRI phase precedes *pP* being a result of the depth of the interface beneath the free surface. We therefore require a specific type of earthquake to use as a candidate source for the detection of a HRI phase—an intraslab earthquake, at sufficient depth beneath the interface for there to be a clear separation between *P* and the HRI phase, and of sufficiently small magnitude (Mw ~4.0–6.0) that the earthquake source (a) can be treated as a point source; (b)

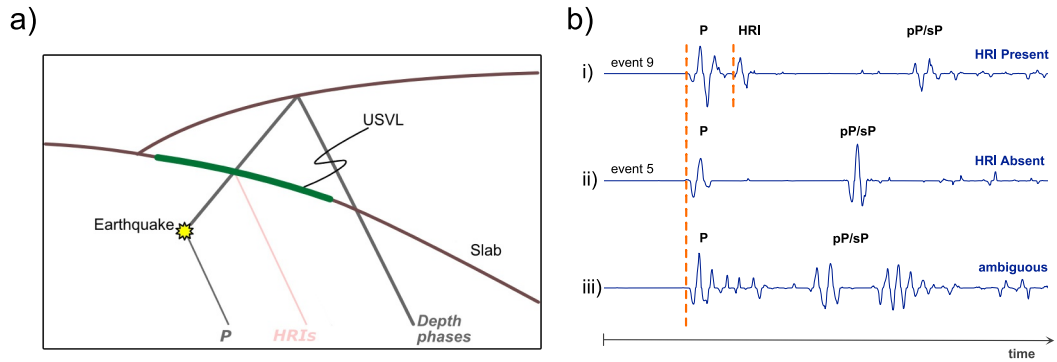

Figure 1. (a) Sketch model illustrating seismic wave propagation: direct P phase, HRI phase reflected from the Ultraslow velocity layer within the slab (target of this study), and depth phases. (b) Stacked waveforms. (i) Example classified as HRI Present, showing a clear secondary arrival between the direct P phase and the depth phases (pP, sP). (ii) Example classified as HRI Absent, with no distinct intermediate reflection. (iii) Example classified as HRI Ambiguous, where potential intermediate energy cannot be robustly separated from the P-wave coda; this example corresponds to the 31 March 2007 event shown in the SI. Event numbers (5 and 9) follow the numbering in Table S1 in Supporting Information S1. Differences in reflected-phase arrival times arise from variations in source depth and source–receiver geometry, which control the bounce-point location.

does not rupture through the slab to the slab surface (the interface); (c) radiates seismic waves dominated by sufficiently high frequencies (0.5–5 Hz) that they are sensitive to relative thin layering in the elastic structure, associated with impedance contrasts at the subduction interface; and (d) is sufficiently far below the interface that the direct arrival and any HRI phase are separated in time by more than the rupture duration of the earthquake source.

Given the small magnitude and the frequency content with which we must work if we hope to detect HRI phases in the seismic record, single-station teleseismic data is unlikely to be sufficient to detect such small-amplitude signals. We therefore use vertical component seismic data from small aperture seismic arrays, beamforming signals based on best azimuth and slowness to boost the signal-to-noise ratio of the direct *P* wave (Figure 2). From the optimal array beam we then first identify the principal depth phase, and then search for any intermediate phase arriving in the window between the end of the direct *P* wave and the depth phase. Following a range of quality-control steps, beams are then classified into three categories—HRI Present, HRI Absent, or HRI Ambiguous. Classification is based on whether the beam envelope is best represented by one or two Gaussian functions (with varying amplitude, width, and center time) within the *P*–*pP* window. Events for which two clearly separated, independent Gaussians are required to fit the enveloped trace are assigned to the HRI Present Category. The number of Gaussian functions used to represent the envelope is selected based on the minimum number required to achieve a stable and reproducible fit across events, rather than through a formal information-criterion test. Additional Gaussians are introduced only if they improve the fit without producing artifacts. This approach helps distinguish genuine reflected phases from source-related complexity. Events are classified as having a confirmed HRI Absent when, after applying all quality control procedures, the beam envelope within the *P*-to-depth-phase window is best fit by a single Gaussian function, with no evidence of a secondary peak that could indicate a HRI phase. In these cases, the waveform is interpreted as containing only the direct P arrival, and any secondary peak in beam power (if present) falls below the detection threshold or is indistinguishable from the main phase. We note that while the waveforms are filtered up to 5 Hz, the current implementation focuses on envelope timing rather than frequency-dependent amplitude variations. A full exploitation of higher-frequency content, including sensitivity to thin-layered structures and interference effects, is left for future work.

Despite careful pre-processing and beamforming, a significant number of event-array pairs do not yield a robust classification into either HRI Present or HRI Absent categories. There are several reasons for this. In some cases, the available data do not meet initial quality thresholds—for example, too few stations in the array, large azimuthal gaps, or poor signal-to-noise ratios—leading to unreliable beamforming results. In particular, many events progress into the processing stage but are not classified because the slowness analysis fails to identify a clear and stable slowness–backazimuth pair, preventing satisfactory beamforming and the identification of clear, coherent signals. In other instances, the complexity of the direct *P* wave or the proximity in time between *P* and

19448007, 2026, 8, Downloaded from https://agupubs.onlinelibrary.wiley.com/doi/10.1029/2026GL121813 by University Of Leeds The Brotherton Library, Wiley Online Library on [15/04/2026]. See the Terms and Conditions (https://onlinelibrary.wiley.com/terms-and-conditions) on Wiley Online Library for rules of use; OA articles are governed by the applicable Creative Commons License

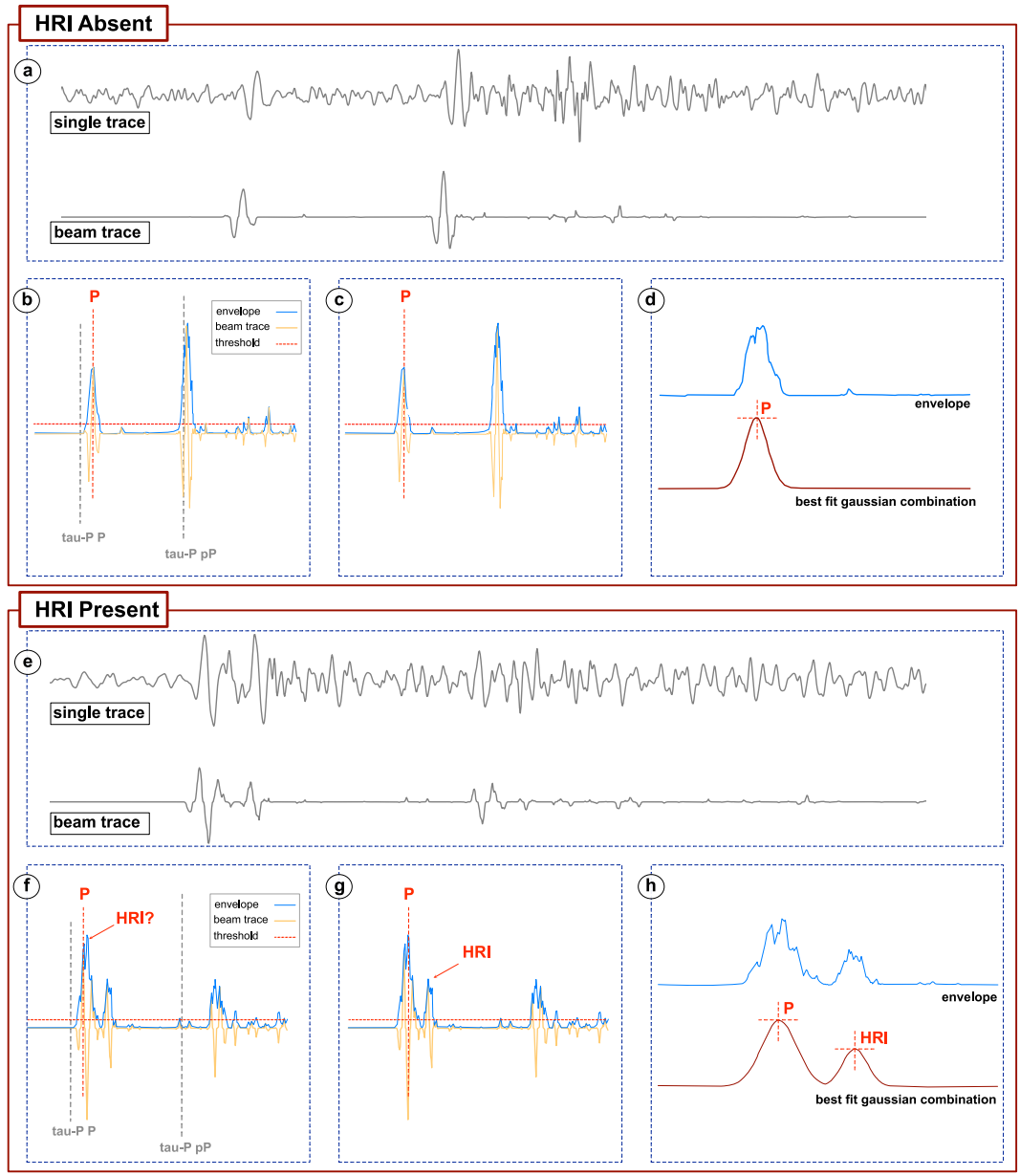

Figure 2. Example of the algorithm applied to a beam trace with (top) and without (bottom) evidence of reflections induced by a Ultraslow velocity layer within the slab. (a) Single trace recorded at an ILAR seismic station (top trace) and the corresponding beam trace (bottom trace), representing the result of beamforming across all ILAR seismic stations. (b) Example of picking. (c) Result of picking after applying the quality check steps. (d) Example of the MGA used for phase identification. (e) Single trace recorded at an ILAR seismic station (top trace) and the corresponding beam trace (bottom trace), representing the result of beamforming across all ILAR seismic stations. (f) Example of picking. (g) Result of picking after applying the quality check steps. (h) Example of the MGA used for phase identification.

the predicted depth phases (e.g., for shallow events or high-frequency content) makes it difficult to resolve any potential intermediate arrivals with confidence. Additionally, overlapping energy from multiple phases or source complexity may distort the waveform envelope such that the fitting algorithm cannot reliably distinguish distinct arrivals—in cases where the source rupture process is anything other than a simple single pulse, source complexity can be indistinguishable from a closely-spaced HRI phase. These cases are classified as HRI Ambiguous, reflecting the limitations imposed by both the data quality and the inherent complexity of teleseismic waveforms. Notably, ambiguous events are retained for further inspection, as some can be reclassified through

19448007, 2026, 8, Downloaded from https://agupubs.onlinelibrary.wiley.com/doi/10.1029/2026GL121813 by University Of Leeds The Brotherton Library, Wiley Online Library on [15/04/2026]. See the Terms and Conditions (https://onlinelibrary.wiley.com/terms-and-conditions) on Wiley Online Library for rules of use; OA articles are governed by the applicable Creative Commons License

19448007, 2026, 8, Downloaded from https://agupubs.onlinelibrary.wiley.com/doi/10.1029/2026GL121813 by University Of Leeds The Brotherton Library, Wiley Online Library on [15/04/2026]. See the Terms and Conditions (https://onlinelibrary.wiley.com/terms-and-conditions) on Wiley Online Library for rules of use; OA articles are governed by the applicable Creative Commons License

manual review. These examples highlight the need for strict quality control and underscore the challenges of automatically detecting subtle seismic phases in global data sets.

A detailed description of the methodology is provided in Text S1 in Supporting Information S1. Figure S1 in Supporting Information S1 summarizes the analysis pipeline for detecting HRI phases. We apply our methodology to the Mexican subduction zone, using data from the Eielson seismic array in Alaska (ILAR; Figure S2a in Supporting Information S1). An additional analysis has been performed for the Chilean subduction zone using the Nevada seismic array (NVAR; Figure S2b in Supporting Information S1), with details provided in Supporting Information S1.

3. Regional Background

Mexico is characterized by a complex tectonic regime dominated by the subduction of the oceanic Cocos and Rivera Plates beneath the North American Plate along the Middle America Trench. This convergent margin extends from central Mexico to Central America, with a convergence rate up to approximately 5 cm/year (Ferrari et al., 2012). Subduction is highly oblique and exhibits significant along-strike variability, influencing both seismic and aseismic deformation processes. In particular, in the Guerrero segment, the subduction interface dips gently and is associated with flat slab geometry at shallow depths (∼30–60 km depth), favoring the accumulation of fluids and the occurrence of SSEs and TT (Husker et al., 2019; Perez-Silva et al., 2021). The presence of a subducted oceanic plateau (e.g., the Orozco Fracture Zone) and heterogeneous slab geometry contribute to segmentation of the megathrust, which plays a key role in the distribution of coupling, SSEs, and large earthquakes. Historically, Mexico has produced large megathrust earthquakes, but also exhibits frequent aseismic slip, making this region a critical natural laboratory for studying the seismic cycle and fluid-mediated fault dynamics in subduction zones.

4. Results and Discussion

Our main case study focuses on the Guerrero region of Mexico. A total of 268 teleseismic events were selected over the period 2000–2022. Of these, 83 events were retained for further analysis, while the remaining were excluded based on a priori criteria (e.g., an insufficient number of available waveforms) which guarantee reliable stacking and robust classification. Of the 83 processed events, 30 were classified as ambiguous due to unresolved phase separation or waveform complexity. Nonetheless, these events were preserved for future visual inspection, as their waveforms may still offer valuable qualitative insights. From the remaining events, only those with a published focal mechanism and independent constraints that reliably define the source characteristics (as extracted from Franco et al. (2020)) were selected for detailed analysis. This final data set includes 24 events with HRI Present and 6 events with HRI Absent, as shown in Figure 3. Waveforms corresponding to events classified as HRI Present, HRI Absent, or HRI Ambiguous are illustrated in Figures S3 and S4 in Supporting Information S1 and their source locations listed in Table S1 in Supporting Information S1. An extended analysis including manually reviewed ambiguous cases is provided in Figure S5 in Supporting Information S1; the main results rely solely on the automated classification.

Events displaying evidence of HRI arrivals form two distinct clusters centered approximately at 17°N and 18°N latitude, elongated in the east-west direction (Figure 3 and Figure S5 in Supporting Information S1). In contrast, events lacking evidence of HRIs are notably fewer. Among them, one (event 6) occurs within the southern group of HRI-associated events, while another (event 5) is located in the transitional area between the two clusters (Transition Zone). The other events (events 1, 2, 3, 4) are found approximately along the margins of the L-SSE- and S-SSE-prone areas.

The two clusters of seismic events with identified HRI phases correspond to well-documented regions associated with L-SSEs and S-SSEs occurring between 2000 and 2020 (El Yousfi et al., 2023; Frank et al., 2015; Radiguet et al., 2016). Major L-SSEs in Guerrero occurred in 2001–2002, 2006, 2009–2010, 2014, 2017–2018, and 2020 (Kostoglodov et al., 2003; Radiguet et al., 2012, 2020). We now consider the temporal variation in HRI phase observations in these two regions separately (Figure 3b). Seismic events with epicenters located within the L-SSE region which show clear HRI phases (orange lines, Figure 3b) are observed in temporal proximity to some of the aseismic events suggesting a potential link between the transient presence of the HRI and the underlying mechanisms driving L-SSEs. In contrast, seismic events in the S-SSE region with clear HRI phases (purple lines, Figure 3b) persist throughout the entire study period (2000–2020), showing little clear correspondence with the

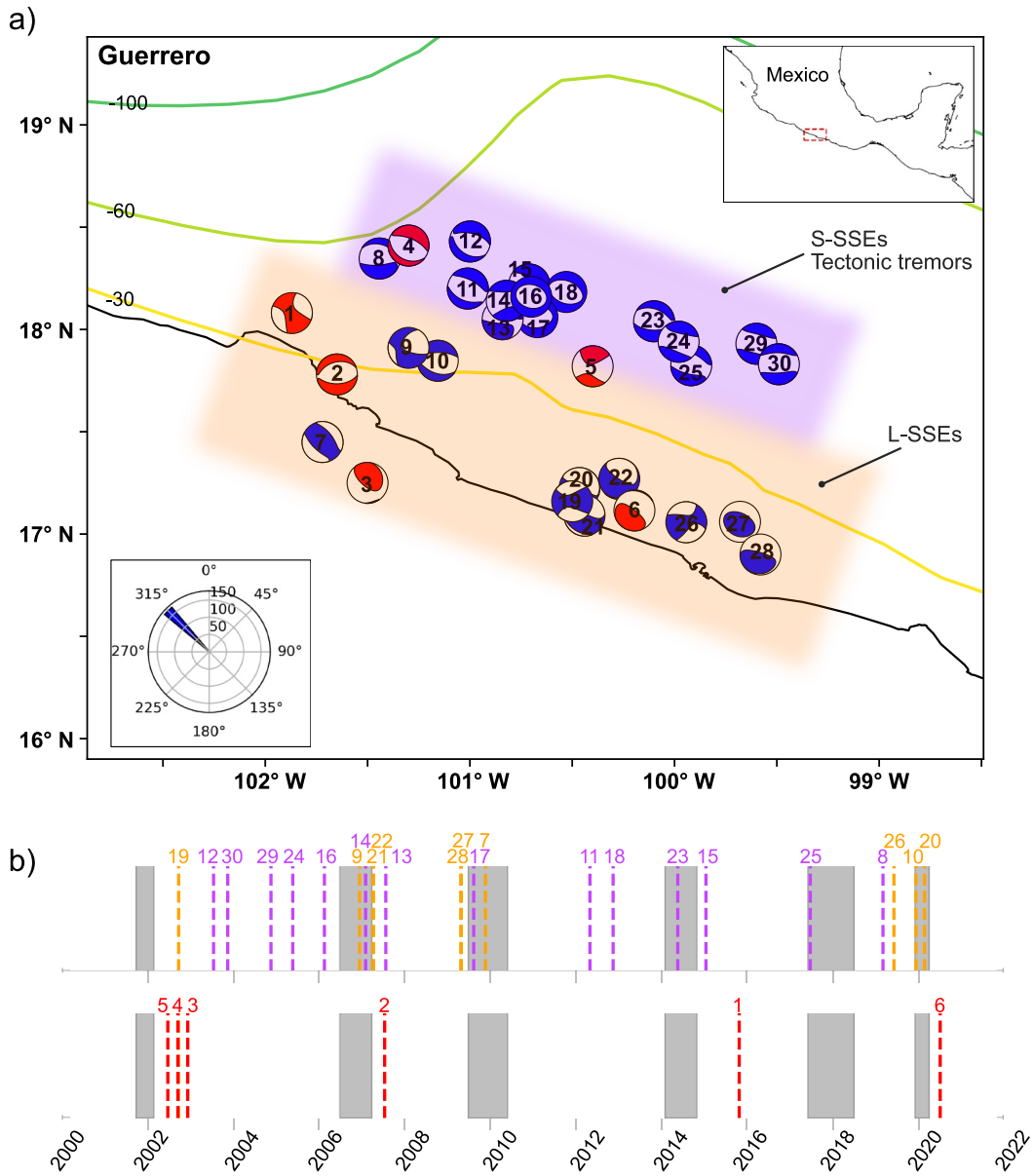

Figure 3. (a) Map of the study area showing focal mechanisms (from Franco et al. (2020)) of events classified based on the presence (blue) or absence (red) of the HRI seismic phase. The region primarily affected by L-SSEs is highlighted in orange, while the area influenced by S-SSEs and tectonic tremor is shown in purple (adapted from (Frank et al., 2015; Husker et al., 2012, 2019; Radiguet et al., 2012, 2016, 2020)). An inset in the lower left corner shows the back-azimuth from the source region to the ILAR array. Colored lines represent slab contours from Slab2 (Hayes et al., 2018). (b) Temporal distribution of the analyzed seismic events. Colored dashed lines indicate events falling in the L-SSE region (orange), S-SSE region (purple), or events with HRI Absent (red). Main L-SSEs are shown as gray bands (adapted from Frank et al. (2015); Radiguet et al. (2016); El Yousfi et al. (2023)). Events characteristics are summarized in Table S1 in Supporting Information S1.

more frequent occurrence of S-SSEs, which recur accompanied by TT activity (Husker et al., 2019; Payero et al., 2008). The consistent presence of HRI reflections in this region suggests a persistent mechanism supporting the regular occurrence of S-SSEs. The two regions therefore exhibit contrasting reflectivity behavior: persistent in the S-SSE area and more variable in the L-SSE region.

To complement these qualitative observations, we quantitatively assessed the relationship between the occurrence of HRI-detecting events and the temporal evolution of SSEs using a contingency analysis. None of the HRI

19448007, 2026, 8, Downloaded from https://agupubs.onlinelibrary.wiley.com/doi/10.1029/2026GL121813 by University Of Leeds The Brotherton Library, Wiley Online Library on [15/04/2026]. See the Terms and Conditions (https://onlinelibrary.wiley.com/terms-and-conditions) on Wiley Online Library for rules of use; OA articles are governed by the applicable Creative Commons License

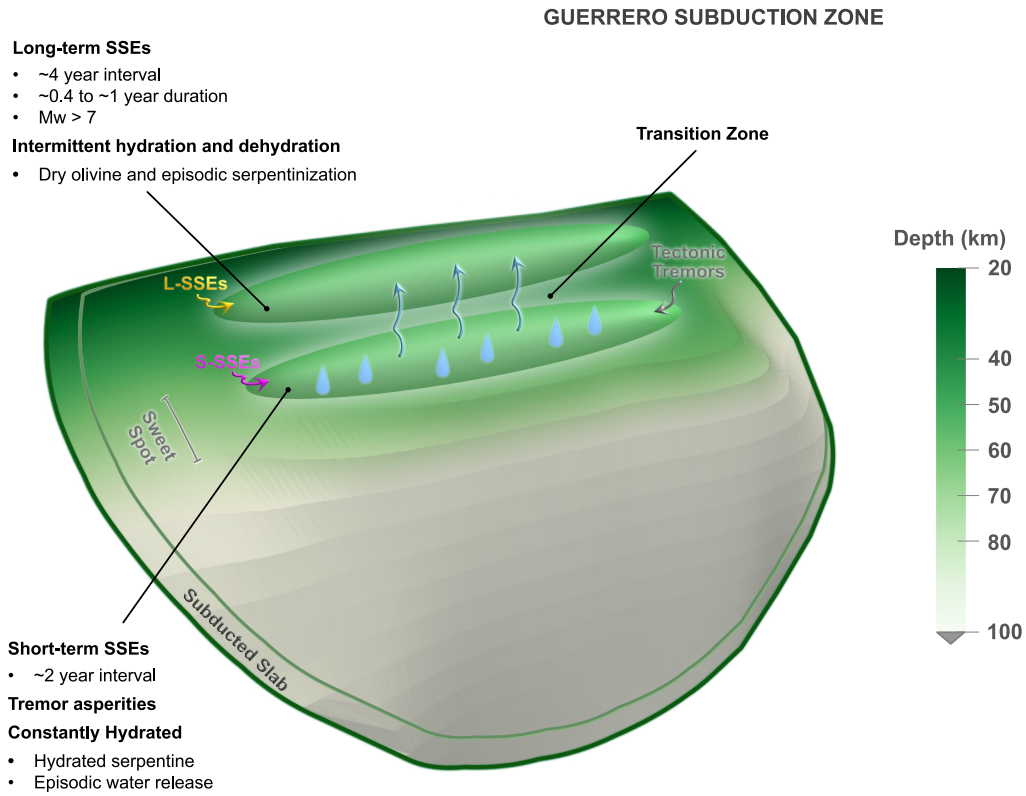

Figure 4. 3-D model of the Guerrero subduction zone, adapted from Slab2 (Hayes et al., 2018). The first ~100 km of the subducting slab highlights two distinct regions: one near the trench, where L-SSEs occur, and another along the flat segment of the slab, where S-SSEs and tectonic tremor are observed.

Absent events occurred during SSE intervals, whereas a subset of the HRI Present events did. A Fisher exact test yields a non-significant p-value ($p = 0.16$), reflecting the limited size of the data set (i.e., 30 events). Although statistical significance is not reached, the absence of HRI Absent events during SSE periods and the preferential occurrence of HRI Present events within SSE intervals (8 events over 24) are consistent with a temporal association between transient megathrust processes and enhanced seismic reflectivity, although this association remains tentative given the limited sample size. Future studies with larger data sets will be required to robustly quantify this relationship.

The observed differences in temporal and spatial distribution may reflect variations in 3-D geometry, properties and fluid dynamics of the subducting slab in Guerrero (Figure 4). Moving downdip (northeastward), from the coast to the inland region, the subduction interface transitions from large to small dip angles as the flat slab region is reached, although the overall inclination remains relatively low throughout (Letort et al., 2018). Perez-Silva et al. (2021) suggest that the shallow-dipping slab segment of the Cocos plate aids the larger magnitudes and longer recurrence interval of the SSEs, concluding that the 3-D slab geometry is an important factor that influences the physics of SSEs. The apparent temporal proximity between some HRI detections and SSEs in the steep portion of the slab near the coast may suggest a transient mechanism influencing fluid flow in this area. The dipping slab (~30 km depth) appears in fact to be characterized by episodic increases in pore pressure, with fluids rising from the deeper "sweet spot"—a section of the flat slab (30–60 km depth) characterized by fluid-rich conditions due to intense slab dehydration—triggering L-SSEs approximately every four years (Cotte et al., 2009; Vergnolle et al., 2010). An increase in pore pressure within the fault zone has been proven to decrease normal stress, promoting slip and increasing nucleation size, favoring slow slip (Bürgmann, 2018; Nakajima & Uchida, 2018). However, given the limited temporal sampling of the present data set, we cannot robustly discriminate between spatial heterogeneity and true time-dependent changes in reflectivity. The proposed link between transient HRI occurrence and L-SSE cycles therefore remains a testable hypothesis. On the other hand,

19448007, 2026, 8, Downloaded from https://agupubs.onlinelibrary.wiley.com/doi/10.1029/2026GL121813 by University Of Leeds The Brotherton Library, Wiley Online Library on [15/04/2026]. See the Terms and Conditions (https://onlinelibrary.wiley.com/terms-and-conditions) on Wiley Online Library for rules of use; OA articles are governed by the applicable Creative Commons License

19448007, 2026, 8, Downloaded from https://agupubs.onlinelibrary.wiley.com/doi/10.1029/2026GL121813 by University Of Leeds The Brotherton Library, Wiley Online Library on [15/04/2026]. See the Terms and Conditions (https://onlinelibrary.wiley.com/terms-and-conditions) on Wiley Online Library for rules of use; OA articles are governed by the applicable Creative Commons License

the continuous presence of the HRI phases from the interface in the flat slab is interpreted to be consistent with a persistently fluid-rich interface in this region, suggesting that the subduction interface (or channel) remains subject to high pore-fluid pressure at all times, substantially weakening it (Audet & Schaeffer, 2018). S-SSE's in this region then reflect either variations in the fault rheology due to periodic water release, or the response of a weak subduction interface to gradually-accumulating tectonic stresses (Bürgmann, 2018). In either case, such conditions would be expected to favor a sustained seismic reflector, consistent with the persistent detection of HRI phases from shallow intraslab events.

Observations of seismic anisotropy in the vicinity of the slab top corroborate the link between fluid presence, high pore pressures, and SSE dynamics, emphasizing the potential of HRIs as a proxy for identifying SSE-prone areas. For example, Husker et al. (2022) observed significant variations in seismic anisotropy within the subducted slab in the Guerrero region, highlighting both spatial and temporal changes in strength and fast wave orientation, corresponding to different slab segments and hydration or dehydration periods. Specifically, the S-SSE region exhibited the highest levels of seismic anisotropy, attributed to the presence of hydrated serpentinite, where phase transitions release water, intensifying anisotropic effects. These anisotropic characteristics have been shown to coincide with elevated pore fluid pressures and increased TT activity (Audet & Kim, 2016; Manea & Manea, 2011), reinforcing the connection between dehydration processes, fluid migration, and transient slip behavior in this region.

Previous seismic imaging studies in central and southern Mexico have consistently documented the presence of a thin, mechanically weak, low-velocity layer at the top of the subducting Cocos plate, particularly within the flat-slab segment of the Guerrero region (Kim et al., 2010, 2012, 2013; Pérez-Campos et al., 2008; Song & Kim, 2012). Receiver-function analyses and migration techniques reveal anomalously low shear velocities, high Vp/Vs ratios, and strong seismic anisotropy within this layer, commonly interpreted as evidence for elevated pore-fluid pressures and talc-rich mineral assemblages that promote decoupling and slow slip.

Our observations are spatially consistent with these previously imaged low-velocity structures, but differ in their observational sensitivity. While receiver-functions are indeed sensitive to impedance contrasts, their reliance on mode conversions and stacking over broad time windows typically constrains the long-term structure of the interface within a limited effective frequency band. In contrast, our approach targets underside P-wave reflections, providing complementary sensitivity to short-wavelength and potentially time-varying impedance contrasts.

The episodic appearance of high-reflectivity arrivals therefore does not imply the formation or disappearance of the low-velocity layer itself, but may reflect temporal modulation of its elastic properties, likely driven by changes in fluid pressure or saturation. In this sense, our results complement existing structural models by providing time-dependent constraints on a well-established weak interface within the Mexican subduction zone.

Synthetic travel-time modeling (Text S2 in Supporting Information S1) demonstrates that the observed $P - P_{ref}$ delays cannot be reproduced by reflections at the crustal Moho. Using TauP ray-tracing (Crotwell et al., 1999), the 1-D velocity model IASP91 (Kennett & Engdahl, 1991) and event-specific source–receiver geometries, we computed predicted delays for both a fixed Moho depth (15 km, following independent receiver-function studies, (Rodríguez-Domínguez et al., 2019)) and a spatially variable Moho extracted from CRUST1.0 (Laske et al., 2012). In both configurations, the Moho predictions systematically overestimate or poorly match the observed delays, whereas models placing the reflector on the subduction interface produce synthetic delays that align closely with both the absolute timing and the observed variability. Bootstrap resampling of the residuals between observed and predicted delays further confirms this result: for a variable Moho, differences between slab and Moho predictions are small and statistically indistinguishable, whereas for a fixed Moho the slab consistently yields smaller residuals, indicating a better fit to the data. These findings support the interpretation that the high-reflectivity phase originates at the plate interface, with the near-zero horizontal offset between source and reflection point reinforcing the robustness of this conclusion. Full details and Figure S6 in Supporting Information S1.

Although other impedance contrasts within the subducting slab or the overriding plate could, in principle, generate reflected phases, several observations are consistent with an origin at the plate interface for the observed HRI arrivals. These include their systematic spatial alignment with the modeled megathrust geometry, the near-

19448007, 2026, 8, Downloaded from https://agupubs.onlinelibrary.wiley.com/doi/10.1029/2026GL121813 by University Of Leeds The Brotherton Library, Wiley Online Library on [15/04/2026]. See the Terms and Conditions (https://onlinelibrary.wiley.com/terms-and-conditions) on Wiley Online Library for rules of use; OA articles are governed by the applicable Creative Commons License

zero horizontal offset between source and reflection point, and their preferential occurrence within regions known to host slow slip.

We emphasize that the present analysis relies primarily on travel-time and envelope characteristics to distinguish potential reflectors. A more detailed waveform-based sensitivity analysis, exploring the effects of layer thickness, impedance contrast, and internal layering on reflection amplitudes, would provide additional constraints on the physical nature of the reflector and represents a natural extension of this work.

Finally, we also applied our detection workflow to intraslab earthquakes along the northern Chile subduction zone (see Text S3 and Figures S7–S9 in Supporting Information S1). Despite the different tectonic environment and data characteristics, the Chilean results display comparable first-orde spatial tendencies as in the Mexican case: HRI phases are preferentially detected in regions of documented slow-slip activity and major megathrust earthquakes (Figures S9 in Supporting Information S1). Although this secondary application is exploratory, it provides an additional illustrative example of how the method performs in a different subduction setting.

5. Conclusions

Our results demonstrate a robust spatial association between high-reflectivity arrivals (HRIs) and regions of documented slow slip in the Guerrero subduction zone, establishing teleseismic underside reflections as a sensitive probe of megathrust reflectivity. This systematic spatial correspondence indicates that these reflections respond to impedance contrasts associated with slow slip–prone megathrust segments. In particular, the S-SSE region exhibits a persistent presence of HRIs, consistent with a mechanically weak, fluid-rich interface previously identified through independent seismic imaging studies. In contrast, HRI detections within the L-SSE region appear more temporally variable. Although the present data set does not allow us to robustly distinguish between spatial heterogeneity and true time-dependent changes in reflectivity, such variability may be consistent with transient modifications of elastic properties along the interface, potentially linked to changes in fluid pressure. We therefore interpret these observations cautiously and view them as motivation for future investigations based on larger and more uniformly sampled data sets. Overall, this work establishes a proof-of-concept framework for remotely probing megathrust reflectivity using teleseismic array data. While continuous temporal monitoring depends on the availability of sufficient intraslab seismicity, the method provides a scalable approach for identifying slow slip–prone regions in offshore subduction zones where geodetic coverage is limited.

Conflict of Interest

The authors declare no conflicts of interest relevant to this study.

Availability Statement

Catalogs of seismic events were retrieved from the International Seismological Centre, On-line Bulletin, (ISC; https://doi.org/10.31905/D808B830), and waveforms from the EarthScope Data Center (IRISDMC; http://service.iris.edu/) as provided by Various Institutions (1965). Information about ILAR and NVAR networks can be found at https://ds.iris.edu/mda/. To access specific metadata, search for "_ILAR" or "_NVAR" within the site.

Acknowledgments
This work was supported by the Leverhulme Trust through Research Grant RPG-2021-336. TJC was supported by the Royal Society under URF\R1\180088, URF\R\231019 and RF\ERE\210041, and also through COMET, which is the NERC Centre for the Observation and Modelling of Earthquakes, Volcanoes and Tectonics. FR acknowledges the ECGS (European Center for Geodynamics and Seismology), which hosted and supported him during the final stages of this study. He also thanks Professor Marco Calò (National Autonomus University of Mexico) for his valuable suggestions regarding the tectonic context of Mexico and for pointing out relevant studies that contributed to this work. The authors thank the editor Germán Prieto and two anonymous reviewers.

References

Audet, P., & Kim, Y. (2016). Teleseismic constraints on the geological environment of deep episodic slow earthquakes in subduction zone forearcs: A review. *Tectonophysics*, *670*, 1–15. https://doi.org/10.1016/j.tecto.2016.01.005

Audet, P., & Schaeffer, A. J. (2018). Fluid pressure and shear zone development over the locked to slow slip region in cascadia. *Science Advances*, *4*(3), eaar2982. https://doi.org/10.1126/sciadv.aar2982

Bürgmann, R. (2018). The geophysics, geology and mechanics of slow fault slip. *Earth and Planetary Science Letters*, *495*, 112–134. https://doi.org/10.1016/j.epsl.2018.04.062

Cotte, N., Walpersdorf, A., Kostoglodov, V., Vergnolle, M., Santiago, J.-A., & Campillo, M. (2009). Anticipating the next large silent earthquake in Mexico. *Eos, Transactions American Geophysical Union*, *90*(21), 181–182. https://doi.org/10.1029/2009eo210002

Crotwell, H. P., Owens, T. J., & Ritsema, J. (1999). The taup toolkit: Flexible seismic travel-time and ray-path utilities. *Seismological Research Letters*, *70*(2), 154–160. https://doi.org/10.1785/gssrl.70.2.154

El Yousfi, Z., Radiguet, M., Rousset, B., Husker, A., Kazachkina, E., & Kostoglodov, V. (2023). Intermittence of transient slow slip in the Mexican subduction zone. *Earth and Planetary Science Letters*, *620*, 118340. https://doi.org/10.1016/j.epsl.2023.118340

Ferrari, L., Orozco-Esquivel, T., Manea, V., & Manea, M. (2012). The dynamic history of the Trans-mexican volcanic belt and the Mexico subduction zone. *Tectonophysics*, *522*, 122–149. https://doi.org/10.1016/j.tecto.2011.09.018

Franco, S. I., Iglesias, A., & Fukuyama, E. (2020). Moment tensor catalog for Mexican earthquakes: Almost two decades of seismicity. *Geofísica Internacional*, *59*(2), 54–80. https://doi.org/10.22201/igeof.00167169p.2020.59.2.2081

Frank, W. B., Shapiro, N. M., Husker, A. L., Kostoglodov, V., Bhat, H. S., & Campillo, M. (2015). Along-fault pore-pressure evolution during a slow-slip event in Guerrero, Mexico. *Earth and Planetary Science Letters*, *413*, 135–143. https://doi.org/10.1016/j.epsl.2014.12.051

Hayes, G. P., Moore, G. L., Portner, D. E., Hearne, M., Flamme, H., Furtney, M., & Smoczyk, G. M. (2018). Slab2, a comprehensive subduction zone geometry model. *Science*, *362*(6410), 58–61. https://doi.org/10.1126/science.aat4723

Husker, A., Castellanos, J. C., Pérez-Campos, X., Valenzuela, R. W., & Frank, W. B. (2022). Crust and upper-mantle seismic anisotropy variations from the Coast to inland in central and southern Mexico (2): Correlations with tectonic tremor. *Geophysical Journal International*, *228*(3), 1713–1723. https://doi.org/10.1093/gji/ggab429

Husker, A., Frank, W. B., Gonzalez, G., Avila, L., Kostoglodov, V., & Kazachkina, E. (2019). Characteristic tectonic tremor activity observed over multiple slow slip cycles in the Mexican subduction zone. *Journal of Geophysical Research: Solid Earth*, *124*(1), 599–608. https://doi.org/10.1029/2018jb016517

Husker, A., Kostoglodov, V., Cruz-Atienza, V. M., Legrand, D., Shapiro, N. M., Payero, J. S., et al. (2012). Temporal variations of non-volcanic tremor (nvt) locations in the Mexican subduction zone: Finding the nvt sweet spot. *Geochemistry, Geophysics, Geosystems*, *13*(3), Q03011. https://doi.org/10.1029/2011gc003916

Ito, Y., Obara, K., Shiomi, K., Sekine, S., & Hirose, H. (2007). Slow earthquakes coincident with episodic tremors and slow slip events. *Science*, *315*(5811), 503–506. https://doi.org/10.1126/science.1134454

Kato, A., & Ben-Zion, Y. (2021). The generation of large earthquakes. *Nature Reviews Earth and Environment*, *2*(1), 26–39. https://doi.org/10.1038/s43017-020-00108-w

Kennett, B., & Engdahl, E. (1991). Traveltimes for global earthquake location and phase identification. *Geophysical Journal International*, *105*(2), 429–465. https://doi.org/10.1111/j.1365-246x.1991.tb06724.x

Kim, Y., Clayton, R., & Jackson, J. (2010). Geometry and seismic properties of the subducting cocos plate in central Mexico. *Journal of Geophysical Research*, *115*(B6), B06310. https://doi.org/10.1029/2009jb006942

Kim, Y., Clayton, R. W., Asimow, P. D., & Jackson, J. M. (2013). Generation of talc in the mantle wedge and its role in subduction dynamics in central Mexico. *Earth and Planetary Science Letters*, *384*, 81–87. https://doi.org/10.1016/j.epsl.2013.10.006

Kim, Y., Miller, M. S., Pearce, F., & Clayton, R. W. (2012). Seismic imaging of the cocos plate subduction zone system in central Mexico. *Geochemistry, Geophysics, Geosystems*, *13*(7), Q07001. https://doi.org/10.1029/2012gc004033

Kostoglodov, V., Singh, S. K., Santiago, J. A., Franco, S. I., Larson, K. M., Lowry, A. R., & Bilham, R. (2003). A large silent earthquake in the Guerrero seismic gap, Mexico. *Geophysical Research Letters*, *30*(15), 1807. https://doi.org/10.1029/2003gl017219

Laske, G., Masters, G., Ma, Z., & Pasyanos, M. E. (2012). Crust1. 0: An updated global model of earth's crust. In *Geophys. Res. Abstr* (Vol. 14).743

Letort, J., Retailleau, L., Boué, P., Radiguet, M., Gardonio, B., Cotton, F., & Campillo, M. (2018). Lateral variations of the Guerrero–Oaxaca subduction zone (Mexico) derived from weak seismicity (m b 3.5+) detected on a single array at teleseismic distance. *Geophysical Journal International*, *213*(2), 1002–1012. https://doi.org/10.1093/gji/ggy035

Manea, V. C., & Manea, M. (2011). Flat-slab thermal structure and evolution beneath central Mexico. *Pure and Applied Geophysics*, *168*(8–9), 1475–1487. https://doi.org/10.1007/s00024-010-0207-9

Nakajima, J., & Uchida, N. (2018). Repeated drainage from megathrusts during episodic slow slip. *Nature Geoscience*, *11*(5), 351–356. https://doi.org/10.1038/s41561-018-0090-z

Obara, K., & Kato, A. (2016). Connecting slow earthquakes to huge earthquakes. *Science*, *353*(6296), 253–257. https://doi.org/10.1126/science.aaf1512

Payero, J. S., Kostoglodov, V., Shapiro, N., Mikumo, T., Iglesias, A., Pérez-Campos, X., & Clayton, R. W. (2008). Nonvolcanic tremor observed in the Mexican subduction zone. *Geophysical Research Letters*, *35*(7), L07305. https://doi.org/10.1029/2007gl032877

Pérez-Campos, X., Kim, Y., Husker, A., Davis, P. M., Clayton, R. W., Iglesias, A., et al. (2008). Horizontal subduction and truncation of the cocos plate beneath central Mexico. *Geophysical Research Letters*, *35*(18), L18303. https://doi.org/10.1029/2008gl035127

Perez-Silva, A., Li, D., Gabriel, A.-A., & Kaneko, Y. (2021). 3d modeling of long-term slow slip events along the flat-slab segment in the Guerrero seismic gap, Mexico. *Geophysical Research Letters*, *48*(13), e2021GL092968. https://doi.org/10.1029/2021gl092968

Radiguet, M., Cotton, F., Vergnolle, M., Campillo, M., Walpersdorf, A., Cotte, N., & Kostoglodov, V. (2012). Slow slip events and strain accumulation in the Guerrero gap, Mexico. *Journal of Geophysical Research*, *117*(B4), B04305. https://doi.org/10.1029/2011jb008801

Radiguet, M., Kazachkina, E., Maubant, L., Cotte, N., Kostoglodov, V., Gualandi, A., & Chanard, K. (2020). Systematic characterization of slow slip events along the Mexican subduction zone from 2000 to 2019. In *Egu general assembly conference abstracts*.17441

Radiguet, M., Perfettini, H., Cotte, N., Gualandi, A., Valette, B., Kostoglodov, V., et al. (2016). Triggering of the 2014 m w 7.3 papanoa earthquake by a slow slip event in Guerrero, Mexico. *Nature Geoscience*, *9*(11), 829–833. https://doi.org/10.1038/ngeo2817

Rodríguez-Domínguez, M., Pérez-Campos, X., Montealegre-Cázares, C., Clayton, R. W., & Cabral-Cano, E. (2019). Crustal structure variations in south-central Mexico from receiver functions. *Geophysical Journal International*, *219*(3), 2174–2186. https://doi.org/10.1093/gji/ggz434

Schwartz, S. Y., & Rokosky, J. M. (2007). Slow slip events and seismic tremor at circum-pacific subduction zones. *Reviews of Geophysics*, *45*(3), RG3004. https://doi.org/10.1029/2006rg000208

Song, T.-R. A., Helmberger, D. V., Brudzinski, M. R., Clayton, R. W., Davis, P., Pérez-Campos, X., & Singh, S. K. (2009). Subducting slab ultra-slow velocity layer coincident with silent earthquakes in southern Mexico. *Science*, *324*(5926), 502–506. https://doi.org/10.1126/science.1167595

Song, T.-R. A., & Kim, Y. (2012). Localized seismic anisotropy associated with long-term slow-slip events beneath southern Mexico. *Geophysical Research Letters*, *39*(9), L09308. https://doi.org/10.1029/2012gl051324

Szeliga, W., Melbourne, T., Santillan, M., & Miller, M. (2008). Gps constraints on 34 slow slip events within the cascadia subduction zone, 1997–2005. *Journal of Geophysical Research*, *113*(B4), B04404. https://doi.org/10.1029/2007jb004948

Various Institutions. (1965). International miscellaneous stations [dataset]. *International Federation of Digital Seismograph Networks*. Retrieved from https://www.fdsn.org/networks/detail/IM/doi:10.7914/VEFQ-VH75

Vergnolle, M., Walpersdorf, A., Kostoglodov, V., Tregoning, P., Santiago, J., Cotte, N., & Franco, S. (2010). Slow slip events in Mexico revised from the processing of 11 year gps observations. *Journal of Geophysical Research*, *115*(B8), B08403. https://doi.org/10.1029/2009jb006852

19448007, 2026, 8, Downloaded from https://agupubs.onlinelibrary.wiley.com/doi/10.1029/2026GL121813 by University Of Leeds The Brotherton Library, Wiley Online Library on [15/04/2026]. See the Terms and Conditions (https://onlinelibrary.wiley.com/terms-and-conditions) on Wiley Online Library for rules of use; OA articles are governed by the applicable Creative Commons License

References From the Supporting Information

Béjar-Pizarro, M., Carrizo, D., Socquet, A., Armijo, R., Barrientos, S., Bondoux, F., et al. (2010). Asperities and barriers on the seismogenic zone in north Chile: State-of-the-art after the 2007 m w 7.7 tocopilla earthquake inferred by gps and insar data. *Geophysical Journal International*, *183*(1), 390–406. https://doi.org/10.1111/j.1365-246x.2010.04748.x

DeMets, C., Gordon, R. G., Argus, D., & Stein, S. (1990). Current plate motions. *Geophysical Journal International*, *101*(2), 425–478. https://doi.org/10.1111/j.1365-246x.1990.tb06579.x

DeMets, C., Gordon, R. G., Argus, D. F., & Stein, S. (1994). Effect of recent revisions to the geomagnetic reversal time scale on estimates of current plate motions. *Geophysical Research Letters*, *21*(20), 2191–2194. https://doi.org/10.1029/94gl02118

Donoso, F., Moreno, M., Ortega-Culaciati, F., Bedford, J., & Benavente, R. (2021). Automatic detection of slow slip events using the picca: Application to Chilean gnss data. *Frontiers in Earth Science*, *9*, 788054. https://doi.org/10.3389/feart.2021.788054

Eckerman, L., Agüero, A., Spagnotto, S., Martinez, P., & Nacif, S. (2018). Seismic-gravimetric analysis of the subducted nazca plate 1 between 32° s and 36° s. *Geodesy and Geodynamics*, *9*(1), 57–66. https://doi.org/10.1016/j.geog.2017.08.002

Herrin, E. T., Negraru, P. T., Golden, P., & Mulcahy, C. (2002). Local site effects at the nevada seismic array (nvar). In *Proceedings of the 24th seismic research symposium, technologies for monitoring the comprehensive nuclear-test-ban treaty* (pp. 17–19). florida.

Hoffmann, F., Metzger, S., Moreno, M., Deng, Z., Sippl, C., Ortega-Culaciati, F., & Oncken, O. (2018). Characterizing afterslip and ground displacement rate increase following the 2014 iquique-pisagua mw 8.1 earthquake, northern Chile. *Journal of Geophysical Research: Solid Earth*, *123*(5), 4171–4192. https://doi.org/10.1002/2017jb014970

Hong, I., Dura, T., Ely, L. L., Horton, B. P., Nelson, A. R., Cisternas, M., et al. (2017). A 600-year-long stratigraphic record of tsunamis in south-central Chile. *The Holocene*, *27*(1), 39–51. https://doi.org/10.1177/0959683616646191

Jara, J., Jolivet, R., Socquet, A., Comte, D., & Norabuena, E. (2024). Detection of slow slip events along the southern Peru - Northern Chile subduction zone. *Seismica*, *3*(1). https://doi.org/10.26443/seismica.v3i1.980

Kanasewich, E., Hemmings, C., & Alpaslan, T. (1973). Nth-root stack nonlinear multichannel filter. *Geophysics*, *38*(2), 327–338. https://doi.org/10.1190/1.1440343

Kendrick, E., Bevis, M., Smalley Jr., R., Brooks, B., Vargas, R. B., Laurıa, E., & Fortes, L. P. S. (2003). The nazca–south America euler vector and its rate of change. *Journal of South American Earth Sciences*, *16*(2), 125–131. https://doi.org/10.1016/s0895-9811(03)00028-2

Klein, E., Duputel, Z., Zigone, D., Vigny, C., Boy, J.-P., Doubre, C., & Meneses, G. (2018). Deep transient slow slip detected by survey gps in the region of Atacama, Chile. *Geophysical Research Letters*, *45*(22), 12–263. https://doi.org/10.1029/2018gl080613

Lindquist, K., Tibuleac, I., & Hansen, R. (2007). A semiautomatic calibration method applied to a small-aperture Alaskan seismic array. *Bulletin of the Seismological Society of America*, *97*(1B), 100–113. https://doi.org/10.1785/0120040119

Muirhead, K. (1968). Eliminating false alarms when detecting seismic events automatically. *Nature*, *217*(5128), 533–534. https://doi.org/10.1038/217533a0

McLaskey, G. C. (2019). Earthquake initiation from laboratory observations and implications for foreshocks. *Journal of Geophysical Research: Solid Earth*, *124*(12), 12882–12904. https://doi.org/10.1029/2019jb018363

Muirhead, K., & Datt, R. (1976). The n-th root process applied to seismic array data. *Geophysical Journal International*, *47*(1), 197–210. https://doi.org/10.1111/j.1365-246x.1976.tb01269.x

Pritchard, M., & Simons, M. (2006). An aseismic slip pulse in northern Chile and along-strike variations in seismogenic behavior. *Journal of Geophysical Research*, *111*(B8), B08405. https://doi.org/10.1029/2006jb004258

Ruiz, S., Metois, M., Fuenzalida, A., Ruiz, J., Leyton, F., Grandin, R., et al. (2014). Intense foreshocks and a slow slip event preceded the 2014 iquique m w 8.1 earthquake. *Science*, *345*(6201), 1165–1169. https://doi.org/10.1126/science.1256074

Schurr, B., Asch, G., Hainzl, S., Bedford, J., Hoechner, A., Palo, M., et al. (2014). Gradual unlocking of plate boundary controlled initiation of the 2014 iquique earthquake. *Nature*, *512*(7514), 299–302. https://doi.org/10.1038/nature13681

Sella, G., Dixon, T., & Mao, A. (2002). Revel: A model for recent plate velocities from space geodesy. *Journal of Geophysical Research*, *107*(B4), 2081. https://doi.org/10.1029/2000jb000033

Socquet, A., Valdes, J. P., Jara, J., Cotton, F., Walpersdorf, A., Cotte, N., et al. (2017). An 8 month slow slip event triggers progressive nucleation of the 2014 Chile megathrust. *Geophysical Research Letters*, *44*(9), 4046–4053. https://doi.org/10.1002/2017gl073023

Wu, S.-M., Pang, G., Koper, K. D., & Euler, G. (2022). A search for large-scale variations in the fine-scale structure of earth's inner core. *Journal of Geophysical Research: Solid Earth*, *127*(9), e2022JB024420. https://doi.org/10.1029/2022jb024420

19448007, 2026, 8, Downloaded from https://agupubs.onlinelibrary.wiley.com/doi/10.1029/2026GL121813 by University Of Leeds The Brotherton Library, Wiley Online Library on [15/04/2026]. See the Terms and Conditions (https://onlinelibrary.wiley.com/terms-and-conditions) on Wiley Online Library for rules of use; OA articles are governed by the applicable Creative Commons License